Consistency of Ion Adsorption and Excess Surface Tension in Molecular Dynamics Simulations of Aqueous Salt Solutions

ARTICLE *in* THE JOURNAL OF PHYSICAL CHEMISTRY C · NOVEMBER 2008

Impact Factor: 4.77 · DOI: 10.1021/jp804811u

3 AUTHORS, INCLUDING:

Daniel J. V. A. dos Santos
University of Lisbon
52 PUBLICATIONS **350** CITATIONS

Consistency of Ion Adsorption and Excess Surface Tension in Molecular Dynamics Simulations of Aqueous Salt Solutions

Daniel J. V. A. dos Santos,[†,‡] Florian Müller-Plathe,[‡] and Volker C. Weiss*[,‡]

iMed.UL, Faculty of Pharmacy, University of Lisbon, Av. Prof. Gama Pinto, 1649-003 Lisbon, Portugal, and Eduard-Zintl-Institut für Anorganische und Physikalische Chemie, Technische Universität Darmstadt, Petersenstrasse 20, 64287 Darmstadt, Germany

Received: May 31, 2008; Revised Manuscript Received: October 1, 2008

Molecular dynamics simulations of the liquid−vapor interface of aqueous solutions of sodium fluoride and of sodium iodide have been carried out using nonpolarizable force fields for ions and water molecules. Despite the absence of explicit polarizability, the tendency of iodide ions to show an enhanced concentration at the surface that was reported for polarizable force fields (Jungwirth, P.; Tobias, D. J. *J. Phys. Chem. B* **2001**, *105*, 10468) is reproduced, while sodium and fluoride ions prefer the interior of the bulk liquid. These observations are confirmed by the contributions of the different species to the surface potential. The systems we study here are much larger than the ones investigated in previous simulations by other authors, which enables us to calculate the adsorption of ions at the interface from the density profiles and subsequently—via Gibbs' adsorption isotherm—the corresponding excess surface tension over that of pure water. The so-obtained values for the surface tension are compared with the results calculated directly from the normal and lateral components of the pressure tensor in the simulation. Consistency is found among the data, but the directly obtained values have significantly larger error bars and are intrinsically more scattered. The Gibbs adsorption isotherm thus not only is a thermodynamic requirement to be met but also offers a reliable and less error-prone way of calculating the surface tension increment from density profiles.

1. Introduction

It is a well-known experimental fact that the dissolution of most inorganic salts in water raises the liquid−vapor interfacial tension beyond that of pure water.[1,2] Early theories[3,4] attempted to explain this phenomenon by appealing to the purely electrostatic picture of charged ions being repelled from the surface by image charges, which, in turn, arise from the abrupt change of the dielectric constant at the liquid−vapor interface. The ions, thus, prefer the bulk solution over the interfacial region. Such a depletion of ions near the interface implies a negative adsorption for these species and, via Gibbs' adsorption isotherm, leads directly to an increase of the surface tension beyond that of pure water. In their classic paper, Onsager and Samaras[4] succeeded in deriving a limiting law for vanishingly low concentration of salt, which is believed to be exact in a way that is completely analogous to the Debye−Hückel limiting law for the activity coefficients of ions in aqueous solution.[5] At finite concentrations, however, an ion specificity is observed experimentally; i.e., different salts will raise the surface tension by different amounts even at the same nominal concentration.[2] These specific effects of ions on the surface tension are caused by, among other properties, their different sizes and polarizabilities.

The phenomenon of ion specificity goes beyond the theoretical framework of Debye−Hückel theory, which assumes cations and anions to be equisized. The fact that a solution of sodium fluoride (NaF) shows a stronger increase of the surface tension than an equimolal solution of sodium iodide (NaI) cannot be explained within Onsager−Samaras theory, unless effective ion diameters are invoked as adjustable parameters. Furthermore, Onsager−Samaras theory predicts identical density profiles for cations and anions and, therefore, no ionic contribution to the surface potential. It has been known for decades that solutions of alkali halides do show a small, but measurable, change of the surface potential as compared to pure water. The sign of this shift suggests that the anions approach the liquid−vapor interface more closely than the cations.[6] Still, based on the density profiles arising within Onsager−Samaras theory, one may expect that the density of both cations and anions varies monotonically from virtually zero at the interface to the bulk value in the liquid phase and that the profiles of anions and cations are merely shifted with respect to each other to produce a surface potential. The net adsorption Γ (to be defined below) must, of course, be the same for both ionic species as required by the condition of electroneutrality of the whole system, i.e., $\Gamma_{\text{cation}} = \Gamma_{\text{anion}} = \Gamma$. Both surface tension measurements as well as surface potential data suggest that bigger, more polarizable ions, such as iodide, are able to come closer to the interface than small, hardly polarizable ions, such as fluoride (or the sodium counterion).

The traditional view of a monotonically varying density profile has been challenged within the past decade. Hu et al. studied the uptake of gaseous Cl_2 and Br_2 by aqueous solutions of NaBr and NaI, respectively.[7] Their kinetic data could only be interpreted successfully if the possibility of a reaction between the halogen gas and a halide ion in solution at the liquid−gas interface was included. For such a reaction to occur, the halide ions in solution must show a considerable surface propensity, at variance with the traditional theoretical picture of the interface. Knipping et al.[8] reported experimental results

* Corresponding author. Present address: Bremen Center for Computational Materials Science, Universität Bremen, Am Fallturm 1, 28359 Bremen, Germany. Tel.: +49 421 218 7762. Fax: +49 421 218 4764. E-mail: volker.weiss@bccms.uni-bremen.de.

† University of Lisbon.

‡ Technische Universität Darmstadt.

10.1021/jp804811u CCC: $40.75
Published on Web 11/14/2008

on the reaction of hydroxyl radicals (generated from ozone in the gas phase) with chloride ions in solution. The formation of chlorine could only be rationalized in the kinetic modeling if a substantial number of chloride ions were able to surface from the bulk solution. In addition, results from molecular dynamics simulations of aqueous NaCl solutions were presented, which corroborated the picture of chloride ions being present at the surface. Further details of the modeling study showing similar results were given by Jungwirth and Tobias.[9] Earlier, Perera and Berkowitz had found, also in a molecular dynamics study, that chloride ions tend to remain on the surface of small water clusters, while the smaller and less polarizable fluoride ion becomes fully hydrated and, accordingly, moves to the interior region of the cluster.[10]

In subsequent simulations of four different sodium halide solutions (fluoride through iodide), Jungwirth and Tobias demonstrated that the propensity of the halide ion for the surface increases with size and polarizability.[11] Fluoride ions stay in the bulk liquid phase, chloride is found at the surface in considerable amounts, while bromide and, even more so, iodide show an even enhanced concentration at the surface as compared to the bulk. At this point, it is worthwhile emphasizing again that all four salts *raise* the surface tension even in the simulations. Jungwirth and Tobias[11] concluded that "...an increase of the surface tension does not necessarily imply negative adsorption of the ions", in apparent contradiction to the Gibbs adsorption isotherm (cf. section 2) and, thus, the laws of thermodynamics. This view was supported by Garrett[12] who suggested that "...cations and anions behave differently and should be treated as separate components", implying a violation of the electroneutrality requirement and of Gibbs' phase rule.

The serious thermodynamic puzzle provided by the results of the simulations of Jungwirth and Tobias, as well as their implications for atmospheric chemistry at the marine boundary, warranted the continued interest of the above-mentioned authors and other researchers—experimentalists, simulators, and theorists alike—in the years to follow.

The first question to be answered by the experimentalists was whether the surface propensity of the heavier halides was real or merely an artifact of the interaction potential (a polarizable force field) used in the simulations. To be able to address this question, techniques that probe the interface at the molecular level directly are needed. Measurements of the surface tension[2,6,13] or the surface potential[6] yield only integral information on the interface rather than the molecular detail required here. Liu et al.[14] as well as Raymond and Richmond[15] used vibrational sum frequency spectroscopy to probe the interfacial water structure of sodium halide solutions. Their conclusions are not unambiguous. Liu et al. find that sodium fluoride and chloride do not alter the structure of the topmost layer of water, suggesting that all the ions in these solutions prefer to stay in the bulk region, while sodium bromide and iodide cause a notable distortion in the water structure, indicating their presence at the surface.[14] The results seen by Raymond and Richmond show no effect of the dissolved salts (NaF, NaCl, NaBr, and NaI) on the topmost layer.[15] Their finding does not explicitly preclude the presence of ions at the surface but shows only that, if there are any, the water structure is unaffected by their presence. The surface-sensitive experiments carried out by Petersen and Saykally on solutions of sodium and potassium halides by means of second harmonic generation spectroscopy remained inconclusive with respect to a possible preferential adsorption of iodide anions to the surface; the lighter halides showed no preference for the interfacial region.[16] Ghosal et al. used X-ray photoelectron spectroscopy to measure the composition of the interfacial region in aqueous solutions of potassium bromide and iodide.[17] Their data indicate a strong enhancement of the iodide concentration at the interface that is even more pronounced than the one found by Jungwirth and Tobias in their simulations.[11] As an aside, Ghosal et al. suggest an improvement of the force field to obtain quantitative agreement. Another method of investigating the surface composition is grazing incidence X-ray fluorescence. Padmanabhan et al. used this technique to study mixtures of alkali halides.[18] Their data provide the first direct evidence that iodide shows a stronger propensity for the interface than chloride, in agreement with the empirical Hofmeister series and simulation results. A related investigation by Kim et al. was devoted to the dissolution of salts in amorphous ice (which, in spite of being solid, features a structure similar to liquid water) and the adsorption of ions onto its surface.[19] By means of low-energy sputtering, reactive ion scattering, and temperature-programmed desorption mass spectrometry, they were able to show that sodium and fluoride ions prefer the interior of the ice sample, while chloride and, even more so, bromide prefer the surface. These findings are in complete qualitative agreement with the situation for liquid water. Summarizing the experimental findings, there can now be hardly any doubt that heavier halide ions are present at the liquid−vapor interface and that their tendency to migrate to the surface increases in the order given by the Hofmeister series: $F^- < Cl^- < Br^- < I^-$.

The conclusions drawn from the direct experimental observations call for a clarification by means of theory and simulation to resolve the apparent contradiction between the relation of the adsorption and the excess surface tension stated by the Gibbs adsorption isotherm and the findings from the simulations of Jungwirth and Tobias.[11] An important issue to be addressed first was the question of an appropriate choice of the force field. In particular, it was of interest to investigate whether polarizability needs to be included explicitly to observe the reported increase of the concentration of heavier halide ions near the surface or if the size of ions alone could lead to similar results. The answer to this question does not seem to be clear-cut but depends on the degree of surface-concentration enhancement that one wishes to achieve. Dang and Chang[20] calculated the potential of mean force for an iodide ion leaving the bulk water phase and crossing the interface into the gas region. Comparing a polarizable force field with a nonpolarizable one, they found that only the former led to a mininum near the interface and, thus, provided the possibility of the ion "binding" to the interface. Extending this study, Dang[21] investigated the corresponding potential of mean force also for bromide and chloride ions, using polarizable potentials in all cases. He found a minimum that was shallower than the one for iodide in the case of bromide but detected no binding of the chloride ion to the liquid−vapor interface. These findings supported the earlier conclusions of Jungwirth, Tobias, and co-workers[8,11] that a polarizable potential was necessary to observe surface enhancement as well as the trend of the surface propensity as the halide ions become more and more polarizable.[22] In 2004, Vrbka et al. reported on a study in which they presented the density profiles for sodium and iodide ions near the liquid−vapor interface for four different potential models.[23] The first one used nonpolarizable force fields for all particles and showed virtually no enhancement of the iodide concentration near the surface. The second force field treated ions as nonpolarizable particles but employed a polarizable water model: a clear enhancement of the iodide concentration was seen at the surface. A similar result was obtained in the third system, in which the ions were polarizable, but water molecules were

not. The strongest surface propensity of iodide ions displayed the fourth system consisting of polarizable ions and polarizable water molecules. The conclusion from this study was that polarizability rather than mere size of the ions caused their presence at the water surface.[23]

It should be mentioned at this point that there are, in principle, infinitely many nonpolarizable potential models for NaI and for water, so what might be true in one particular model (or combination of models) may be different in another one. Patra and Karttunen[24] compared several force fields widely used to simulate aqueous solutions of NaCl and found that differences in the force-field parameters could be as large as 10% for the radius and 50% for the depth of the attractive Lennard-Jones potential well. These differences are caused by the quality and the availability of experimental data to be used for fitting the parameters. Particularly in the case of ions, another mismatch exists if one is interested in solutions of finite concentration because the parameter fitting is usually done for the infinitely dilute regime. An additional problem for systems with interfaces arises from the fact that force fields are usually parametrized by matching bulk properties (e.g., densities, free energies of solvation, radial distribution functions) which can be very different from the properties near interfaces. For all of these reasons, it is no surprise that the force-field parameters and, consequently, the quality of the simulated results may vary significantly.

Having seen the importance of polarizabilities for the surface propensity of ions, it must be mentioned that the results of other studies indicated that an enhanced surface concentration of anions could be produced by the size effect alone, i.e., without the explicit inclusion of polarizability. Bhatt et al.[25,26] reported a positive adsorption of NaBr and NaCl at higher concentrations despite using a nonpolarizable potential. Kalra et al.[27] studied the preferential interaction of different anions with a hydrophobic solute particle in water, while Pal and Müller-Plathe[28] investigated the adsorption of anions from an aqueous solution to a hydrophobic surface (an alkane crystal instead of a liquid−vapor interface). Both studies concluded that size alone was sufficient to see a preference of the bigger ions for the surface of the hydrophobe. Most recently, Eggimann and Siepmann[29] simulated mixtures of nonpolarizable spherical anions of different sizes (with counterions all being the same size) and observed that bigger ions show a stronger tendency to be found at the interface than small ones. In view of the above results, it is fair to conclude that both size and polarizability influence the surface propensity of an ion and that an experimentally observed adsorption can be reproduced even by a nonpolarizable force field if other parameters are chosen accordingly.

With the existence of an enhancement of the anion concentration at the surface being confirmed by experiments and after clarification of the important ingredients of a force field to model salt solutions showing the above effect, one may now address the fundamental thermodynamic issue raised by the simulations of Jungwirth and Tobias:[11] How can the observed enhanced concentration of the heavier halide anions at the surface be reconciled with an increase of the surface tension? The key to answering this question is found in the Gibbs adsorption isotherm itself. A brief summary of the most important considerations that lead directly from the foundations of thermodynamics, namely, the first and the second laws, to Gibbs' adsorption equation is found in the Appendix. Choosing the Gibbs dividing surface in such a way that the adsorption Γ_w of the solvent (water) becomes zero, the Gibbs adsorption isotherm relates the adsorption of the solute (salt) Γ to the infinitesimal change of the surface tension γ of the mixture[30]

$$d\gamma = -RT\Gamma d \ln a = -\frac{RT}{a}\Gamma da \tag{1}$$

where T denotes the temperature, R is the universal gas constant, and a is the activity of the ions. The activity a may be written as the product of the molality m and the activity coefficient f. For ideal-dilute solutions, one has $f = 1$, and eq 1 may be simplified and rearranged into the more suggestive form

$$\Gamma \approx -\frac{m}{RT}\frac{d\gamma}{dm} \tag{2}$$

It is this last equation that leads to the statement that a positive adsorption implies a decrease of the surface tension with increasing solute concentration, while a negative value of Γ causes an increase of γ. The apparently positive adsorption of iodide at the surface, therefore, contradicts the observed increase of the surface tension.[11] There are two flaws in this conclusion. The first one was noted by Bhatt et al.,[25,26] the second one by Vrbka et al.[23] (i.e., by Jungwirth and Tobias themselves). Bhatt et al.[25] pointed out that eq 1 and, consequently, eq 2 concern the infinitesimal variation of γ as a or m, respectively, are changed. It is, thus, conceivable that if Γ is negative at low solute concentration and turns positive for larger m the surface tension at that higher concentration, $\gamma(m)$, might still be larger than $\gamma(0)$ for the pure solvent even though $\Gamma(m)$ is positive;[25] only the slope of $\gamma(m)$ will be negative at this concentration if $\Gamma(m)$ is positive. For the above scenario of a Γ that is negative for small m but positive for larger m, the Gibbs adsorption isotherm implies the existence of a maximum of $\gamma(m)$. Such a maximum was indeed found by Bhatt et al.[26] in their simulations: from their (rather noisy) density profiles for NaCl and NaBr, they calculated the adsorption (with considerable error bars) at different concentrations and found it to be negative at small m but positive at larger m. They concluded that the occurrence of such peculiar behavior casts doubt on the validity of the force fields they used because the excess surface tensions (over that of pure water) for the real counterparts of these salt solutions increase monotonically (and almost perfectly linearly) with m over the entire range of possible solute concentrations. Vrbka et al.[23] realized that an enhancement of the (an)ion concentration at the surface does not necessarily imply a positive *overall* adsorption of the salt (or of just one ionic species). To determine the adsorption, the entire interfacial region needs to be taken into account, and it is seen in the simulations that the peak at the surface is followed by a depletion (as compared to the bulk density) of the ions. The integrated adsorption Γ may thus be negative and in agreement with the increase of the surface tension over that of pure water, which also Jungwirth and Tobias had found.[11] In this and later papers,[31] however, Jungwirth, Tobias, and co-workers did not attempt to calculate the adsorption from their density profiles because their systems were too small to produce true bulk-phase behavior in the liquid; i.e., their density profiles never leveled off to the density of the bulk liquid. In addition, they refrained from (over)interpreting the calculated excess surface tension due to the considerable uncertainty, which they estimated to be at least 1 mN m^{-1}.[32] The observed trends for different halide ions, however, correspond to the experimental findings.[11,33]

The first attempt to compare the adsorption as calculated from density profiles obtained in simulations to the experimentally determined adsorption (which can be deduced from eq 1 using experimental data for the surface tension and the activity

coefficient) was made by Ishiyama and Morita.[34] Using their newly developed polarizable force field (which reproduced the enhanced concentration of iodide near the surface), they calculated the adsorption for model NaCl and NaI and found both of them to be too large (i.e., not negative enough) as compared to the experimental adsorptions. Unfortunately, Ishiyama and Morita did not calculate the excess surface tension over that of pure water as a function of the salt concentration in their simulations. It was concluded that important issues to be addressed in future studies were the system-size dependence of Γ as well as the search for a force field that correctly reproduces the experimental adsorption. More recently, Warren and Patel[35] compared simulation results obtained from polarizable and nonpolarizable models of solutions of NaCl and NaI. In line with earlier studies, they showed that polarizability enhances the surface propensity of anions but that an increased iodide concentration is also found in the nonpolarizable model. Like Ishiyama and Morita, Warren and Patel calculated the adsorption of ions at the interface but did not study the effect on the surface tension. They concluded that systems of at least twice the size that they had chosen would be needed to obtain reliable results.

The purpose of our present contribution is three-fold. First, we extend the simulations to large enough system sizes so as to find bulk behavior in the interior of the liquid phase. The size needed to ensure this feature is so large that we have to use nonpolarizable force fields. We then calculate the adsorption and, independently, the surface tension for different concentrations of two salts, namely, NaF and NaI. For the latter, we employ two different force fields to compare the consistency of adsorption and surface tension with the Gibbs adsorption isotherm and to investigate the occurrence and the importance of a surface peak of the anion concentration in this respect. Third and, to the best of our knowledge, for the first time for aqueous solutions of alkali halides, we derive the excess surface tension from the adsorption and compare it with the directly calculated values.[36]

In the following section, we give the simulation details and explain the methodologies used to deduce the adsorption data and to estimate the surface tension increments based on these adsorptions. In section 3, we show the density profiles resulting from our simulations and the properties that were calculated from them. A discussion of the consistency of these results is also given in this section. Section 4 concludes the paper, summarizes the significance of our findings, and attempts to give suggestions for future research.

2. Simulation Details and Methodology

2.1. Details of the Simulations. The GROMACS 3.3.1 package[37] was used to simulate aqueous solutions of NaF and NaI at four different concentrations.

The initial bulk system was set up by arranging 3612 flexible SPC/E water molecules, 400 cations (Na^+), and 400 anions (I^-) to occupy the sites of a simple cubic lattice in a molecular dynamics simulation box with periodic boundary conditions applied in all directions. The ions were modeled by the OPLS force field (cf. Table 1). This system was then allowed to relax first at *NVT* conditions (for a few tens of picoseconds with a target temperature of 300 K) and, afterward, in the *NPT* ensemble using an anisotropic pressure coupling to treat the *x* and *y*-components of the pressure separately from the *z*-component. This procedure is adopted to obtain box dimensions in the *x*- and *y*-direction of slightly more than 30 Å.

After reaching this target interface area of about 30 × 30 Å^2, additional time for equilibration in the *NPT* ensemble under isotropic pressure-coupling conditions was allowed until the system reached equilibrium. Only then a certain number of ions was removed to obtain four bulk systems with different target molarities of 0.5, 1.0, 2.0, and 4.0 mol L^{-1} (an iteration based on equilibration, production, and removal of ions was needed to get the systems to the target concentrations). The final four bulk systems contained 33, 70, 144, and 330 ion pairs, respectively.

Two liquid−vapor interfaces were created in each of these four bulk systems by increasing the length of the simulation box in the *z*-direction (cf. Figure 1) and performing a final equilibration run in the *NVT* ensemble for no less than 100 ns. As an example, Figure 2 shows the density profiles of the different constituents in the simulation box which is replicated using periodic boundary conditions. In these systems, the box length in the *z*-direction (i.e., perpendicular to the interface), L_z, is 190 Å, while the interface has an area of about $L_x \times L_y$

TABLE 1: Lennard-Jones Parameters for the Ionic Force Fields Used in the Simulations[a]

	OPLS		Koneshan et al.[43]	
ion	σ (Å)	ε (kJ mol^{-1})	σ (Å)	ε (kJ mol^{-1})
Na^+	3.330	0.01160	2.610	0.4184
F^-	2.733	3.0125	---	---
I^-	5.400	0.2929	5.482	0.4184

[a] For the OPLS force field, the Na^+ parameters are taken from Åqvist,[38] and the parameters for I^- and F^- are adopted from Jorgensen and collaborators.[39,40]

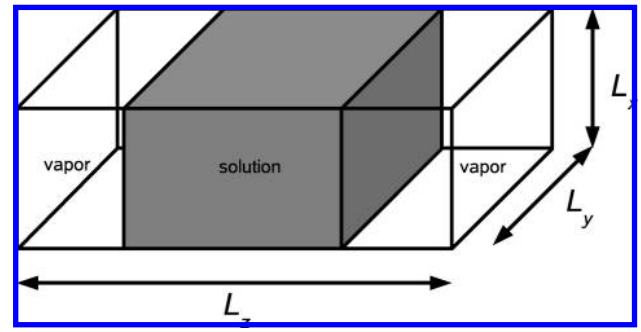

Figure 1. Molecular dynamics simulation box showing the two liquid−vapor interfaces with the liquid slab (shaded) in the middle and vapor regions at either side. In all systems studied, $L_z = 190$ Å and $L_x = L_y \approx 30$ Å.

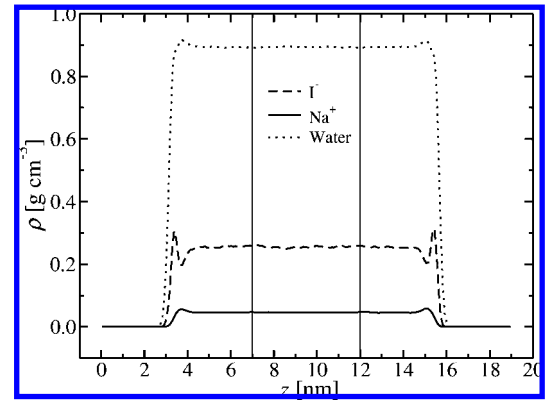

Figure 2. Density profiles for the NaI system (OPLS force field) at a molality of $m = 2.215$ mol kg^{-1}. Displayed are the mass densities of the ions and of water. The length of the box in the *z*-direction is 190 Å. For determination of the bulk densities of the different species in the liquid phase, the region between $z = 7$ nm and $z = 12$ nm, indicated by two vertical lines, is used.

TABLE 2: Water Density ρ_w and Mass Density of the Entire Solution ρ for Different Salts, Force Fields, and Concentrations m[a]

NaF	OPLS		
m (mol kg^{-1})	ρ_w (particles nm^{-3})	ρ (g cm^{-3})	ρ_{expt} (g cm^{-3})
0.492	33.89	1.0358	1.017
0.984	34.14	1.0662	1.038
1.969	34.53	1.1244	1.081*
3.845	34.94	1.2289	1.167*
NaI	OPLS		
m (mol kg^{-1})	ρ_w (particles nm^{-3})	ρ (g cm^{-3})	ρ_{expt} (g cm^{-3})
0.508	32.76	1.0553	1.053
1.077	31.86	1.1090	1.113
2.215	30.16	1.2062	1.227
5.076	26.48	1.4020	1.472
NaI	Koneshan et al.		
m (mol kg^{-1})	ρ_w (particles nm^{-3})	ρ (g cm^{-3})	ρ_{expt} (g cm^{-3})
0.508	32.69	1.0528	1.053
1.077	31.72	1.1040	1.113
2.215	29.93	1.1966	1.227
5.076	26.16	1.3845	1.472

[a] The experimental mass densities of the solutions, ρ_{expt}, are also given.[41] The starred data for NaF are extrapolated beyond the solubility limit. The density of pure water in the simulations is 33.57 particles nm^{-3} or 1.0034 g cm^{-3}, to be compared with the experimental value of 0.9966 g cm^{-3}.[42]

$= 30 \times 30$ Å^2. The total thickness of the liquid slab is about 130 Å, of which 50 Å are bulk solution, while the distance between the two liquid−vapor interfaces is about 60 Å through the space occupied by the vapor phase.

We used the four different NaI bulk systems to build the NaF systems by changing the iodide potential to the fluoride one (OPLS force fields, cf. Table 1)[38−40] and by adjusting the number of NaF ion pairs. The desired number of NaF ion pairs was obtained in a similar deletion procedure as applied for NaI to get the systems to the four target molarities (0.5, 1.0, 2.0, 4.0 mol L^{-1}). The final systems contained 32, 64, 128, and 250 ion pairs, respectively. After some equilibration time, a similar procedure as decribed above was then applied to establish two liquid−vapor interfaces in each of these four systems. A final equilibration run in the *NVT* ensemble of no less than 100 ns followed. The systems obtained in this way have molalities of 0.492, 0.984, 1.969, and 3.845 mol kg^{-1} for NaF and of 0.508, 1.077, 2.215, and 5.076 mol kg^{-1} for NaI. The resulting bulk densities of the liquid phase are listed in Table 2 and compared to the corresponding experimental values at atmospheric pressure.[41,42] Good agreement is found for pure water and for the solutions of NaI, while the data for solutions of NaF are still reasonable and reproduce the structure-making effect of this salt by means of which the water density (i.e., not only the overall mass density) increases with increasing salt concentration.

Starting from the four equilibrated aqueous NaI solutions forming two interfaces with the adjacent vapor phase, a second set of four aqueous NaI systems was obtained by first changing the OPLS potential to the one proposed by Koneshan et al.[43] (cf. Table 1) and by equilibrating these new systems for at least 10 ns. By changing the potential, the volume of the solution also changes (especially for the systems of higher salt concentration). We, therefore, decided to report the concentrations in molalities and, consequently, avoid any ion pair adjustment to correct for the target molarities.

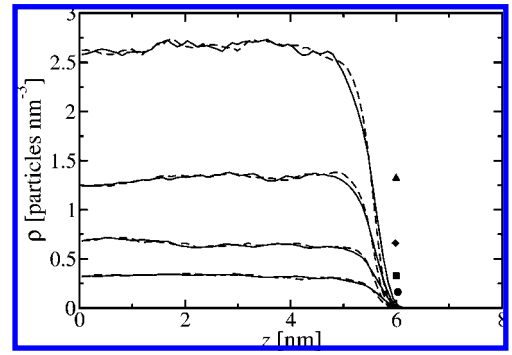

Figure 3. Density profiles for NaF at four different concentrations. From bottom to top: $m = 0.492$ mol kg^{-1}, 0.984 mol kg^{-1}, 1.969 mol kg^{-1}, and 3.845 mol kg^{-1}. Sodium profiles are shown as continuous lines, fluoride profiles as dashed lines. The respective locations of the Gibbs dividing surface, z_{Gibbs}, are indicated by symbols (in order of increasing m by a circle, a square, a diamond, and a triangle), which, just for the graphical representation, have arbitrarily been placed at half the bulk density of the ions in the liquid phase at the corresponding concentration (there is, however, no physical meaning to the position on the ρ-axis in this case).

The 12 systems were simulated for 100 ns in the *NVT* ensemble at $T = 300$ K with a time step of 2 fs to calculate all thermodynamic properties based on the simulations reported here. The flexible SPC/E water model (featuring a harmonic bending potential) included in GROMACS was used,[44,45] which allows for changes of the molecular angle but not of the O−H bond lengths. The latter were kept fixed using the SETTLE algorithm.[46] The use of a flexible water model incorporates the possibility of a modified dipole moment of molecules at the interface, which, however, we did not study in detail.

To keep the temperature constant at 300 K, a Nosé-Hoover thermostat[47,48] with a coupling constant of 0.1 ps was used. A particle mesh Ewald scheme[49,50] was employed to calculate the electrostatic interactions with a cutoff radius of 10 Å for the real space. The same cutoff was applied for the short-range van der Waals interactions. The standard geometric combination rules for the OPLS model were used to obtain the Lennard-Jones parameters between atoms of different species in both sets of potential parameters (cf. Table 1). The OPLS parameters were chosen because they are the default in the OPLS force field distributed with the GROMACS package, and the Koneshan et al. parameters were selected since they had already been used in our group to simulate other interfacial systems with good results.[28]

The positions of the particles were recorded every 500 steps (i.e., at each picosecond) and later analyzed using our own programs (written in C++, using the GROMACS library interface) whenever the respective tool was unavailable in the GROMACS package. The different components of the energy (namely, short- and long-range) were recorded at every 20th time step and used to monitor the evolution of the energetic and dynamic properties (box-size changes, and, especially, the components regarding the interaction between ions and between ions and water molecules for the short- and long-range interactions) and to calculate the surface tension.

The average surface tension γ was calculated from the difference between the normal and the lateral components of the pressure tensor (Kirkwood−Buff formula)[30]

$$\gamma(t) = \frac{1}{n}\int_0^{L_z}\left[P_{zz}(z,t) - \frac{P_{xx}(z,t)+P_{yy}(z,t)}{2}\right]\mathrm{d}z \quad (3)$$

$$\gamma = \frac{L_z}{n}\left\langle P_{zz} - \frac{P_{xx}+P_{yy}}{2}\right\rangle \quad (4)$$

where n is the number of interfaces (2 in our case, cf. Figure 1); L_z is the box length in the z-direction, i.e., perpendicular to the interfaces; P_{xx}, P_{yy}, and P_{zz} are the components of the pressure tensor; and the angular brackets denote an ensemble average.

The surface tension for pure SPC/E water (flexible model) was found to be 59.90 ± 1.26 mN m^{-1}, which is compatible with the value of 61.3 ± 1.5 mN m^{-1} calculated by Chen and Smith for the rigid version of this model.[51]

The error bars reported here were calculated by estimating the decorrelation time D of a property x (the surface tension, for instance) and assuming that complete decorrelation has occurred when the autocorrelation function C of this property

$$C(t) = \frac{\langle (x(t)-\bar{x})(x(0)-\bar{x})\rangle}{\langle (x(0)-\bar{x})^2\rangle} \quad (5)$$

has decayed to zero ($\bar{x} = \langle x\rangle$ denotes an ensemble average of the property x). With this decorrelation time, the standard deviation of the mean can be calculated according to

$$\sigma_{\mathrm{mean}} = \frac{\sigma}{\sqrt{\frac{N}{D-1}}} \quad (6)$$

where σ and N are the standard deviation and the total number of values in the time series, respectively. The standard deviation of the mean is the reported error.

Orea et al. have shown that the surface tension as obtained from simulations can be an oscillatory function of the surface area.[52] However, if the surface area is big enough, the surface tension can be calculated reliably: their results show that, for Lennard-Jones and square-well fluids, the oscillatory behavior is damped rapidly and converges for values of L_x and L_y larger than 7 reduced units of length, which amounts to about 22 Å in our systems of interest, in which the unit length is set by the Lennard-Jones diameter of the oxygen atom in SPC/E water. Moreover, simulations of pure SPC/E water using a system of 500 water molecules and $L_x = L_y = 19.7$ Å or a larger system of 1000 molecules and $L_x = L_y = 23$ Å resulted in essentially no differences in the calculated surface tensions.[53] We, therefore, expect that our calculations for systems containing more than 3600 water molecules and having lateral dimensions of 30 Å will not suffer from the artifacts observed for small systems.

The reported simulations are a considerable computational task because the use of the Gibbs adsorption isotherm requires large systems containing a sufficiently thick slab of the liquid phase. Moreover, long simulation times are needed to calculate the surface tension with good accuracy. The sum of all production runs (not accounting for the equilibration period which is longer than the production part) is 1.3 μs in simulation time, amounting to almost a year in real time on a state-of-the-art AMD single CPU dual core computer.

The density profiles for the ionic species obtained at four different concentrations and accumulated from the two liquid−vapor interfaces are shown in Figures 3−5, namely, for NaF within the OPLS force field in Figure 3, for NaI described by the OPLS force field in Figure 4, and for an alternative NaI force field derived by Koneshan et al. in Figure 5. These profiles will be discussed in section 3 together with results for the adsorption and the surface tension increment.

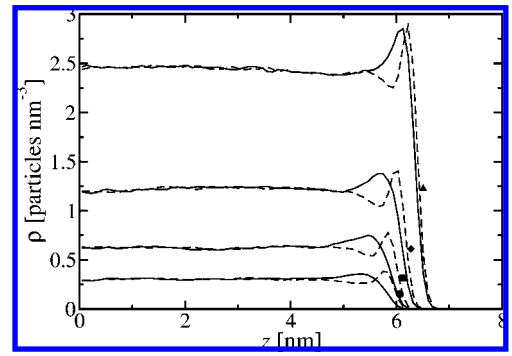

Figure 4. Density profiles for NaI (OPLS force field) at four different concentrations. From bottom to top: $m = 0.508$ mol kg^{-1}, 1.077 mol kg^{-1}, 2.215 mol kg^{-1}, and 5.076 mol kg^{-1}. Sodium profiles are shown as continuous lines, iodide profiles as dashed lines. The respective locations of the Gibbs dividing surface, z_{Gibbs}, are indicated by symbols (in order of increasing m by a circle, a square, a diamond, and a triangle) as described in the caption of Figure 3.

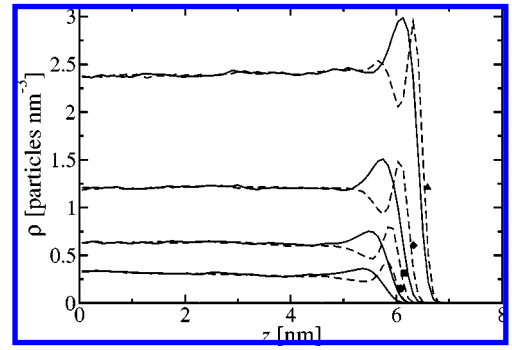

Figure 5. Density profiles for NaI (Koneshan et al. force field) at four different concentrations. From bottom to top: $m = 0.508$ mol kg^{-1}, 1.077 mol kg^{-1}, 2.215 mol kg^{-1}, and 5.076 mol kg^{-1}. Sodium profiles are shown as continuous lines, iodide profiles as dashed lines. The respective locations of the Gibbs dividing surface, z_{Gibbs}, are indicated by symbols (in order of increasing m by a circle, a square, a diamond, and a triangle) as described in the caption of Figure 3.

2.2. Methodologies of Simulation Data Evaluation and Comparison to Experimental Data. Experimental surface-tension data were taken from the extensive study by Matubayasi et al.[13] The adsorption of ions, Γ, can be obtained from these surface tension data using experimental activity coefficients[42] in the following way: Inserting $a(m) = f(m)\cdot m$ for the activity and using the chain rule, the Gibbs adsorption isotherm, eq 1, may be written as

$$\Gamma = -\frac{a}{RT}\frac{d\gamma}{da} = -\frac{fm}{RT}\frac{d\gamma}{dm}\frac{dm}{da} \quad (7)$$

$$= -\frac{fm}{RT}\left(f + m\frac{df}{dm}\right)^{-1}\frac{d\gamma}{dm} \quad (8)$$

where all derivatives are understood to be taken at constant temperature. The required expressions for $\gamma(m)$ and $f(m)$ are obtained by fitting polynomials to the available experimental data. The data of $\Gamma(m)$ for NaF and NaI derived from experiments are shown in Figures 6, 7, and 8 for comparison with the results of our simulations. From eq 8, it becomes clear why eq 2 is applicable not only to ideal-dilute solutions of, say, $m < 0.001$ mol kg^{-1} but also, as a matter of fact, to solutions up to $m \approx 1$ mol kg^{-1}. The actual condition to be met in order for eq 2 to be accurate is not $f \approx 1$, but $f \gg m(df/dm)$, which is the case in a much broader range of concentrations.

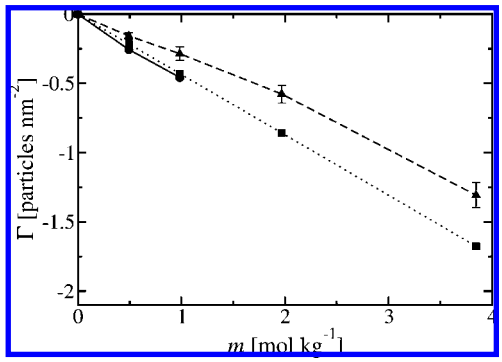

Figure 6. Adsorption Γ for NaF as a function of molality m. Shown are the data deduced from experiments using the actual activity coefficients (circles, solid line) and those obtained when assuming an ideal-dilute solution and linearly extrapolating the surface tension data (squares, dotted line). The results of our simulations are represented by triangles and connected by a dashed line.

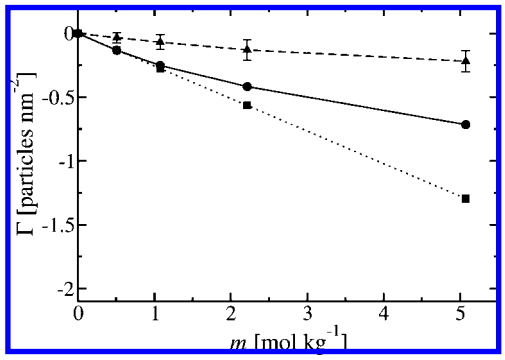

Figure 7. Adsorption Γ for NaI (OPLS potential) as a function of molality m. Shown are the data deduced from experiments using the actual activity coefficients (circles, solid line) and those obtained when assuming an ideal-dilute solution and linearly extrapolating the surface tension data (squares, dotted line). The results of our simulations are represented by triangles and connected by a dashed line.

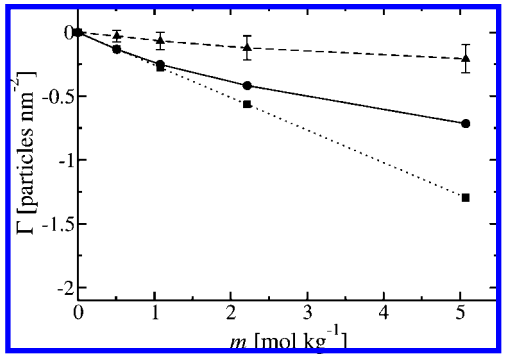

Figure 8. Adsorption Γ for NaI (Koneshan et al. force field) as a function of molality m. Shown are the data deduced from experiments using the actual activity coefficients (circles, solid line) and those obtained when assuming an ideal-dilute solution and linearly extrapolating the surface tension data (squares, dotted line). The results of our simulations are represented by triangles and connected by a dashed line.

To analyze the density profiles resulting from our simulations (which are shown in Figures 3−5) in terms of the adsorption of ions, we first have to locate the Gibbs dividing surface in such a way that the adsorption of the solvent (water) becomes zero. To this end, we describe the water profiles (not shown) for each salt concentration by a least-squares fit to a hyperbolic-tangent profile of the form

$$\rho(z) = \frac{\rho_l}{2}\left[1 - \tanh\left(\frac{z - z_{\mathrm{Gibbs}}}{d}\right)\right] \quad (9)$$

where ρ_l denotes the bulk water density in the liquid phase, z_{Gibbs} is the position of the Gibbs dividing surface on the z-axis, which is perpendicular to the liquid−vapor interface, and d is a measure of the interfacial thickness, the numerical value of which is immaterial here. In using eq 9, the water density in the vapor phase has been neglected since $\rho_v \approx 0$. The symmetry of the hyperbolic-tangent function ensures that Γ_w is zero if z_{Gibbs} is identified with the position of the Gibbs dividing (or equimolar) surface. Once the Gibbs dividing surface has been located, one may compute the adsorption of the ions with respect to this choice of z_{Gibbs}. From the density profile of the ionic species i, $\rho_i(z)$, the adsorption Γ_i is obtained by numerical integration, using the following definition of Γ_i[30]

$$\Gamma_i = \int_{-\infty}^{0} [\rho_i(\hat{z}) - \rho_{i,\mathrm{liq}}]\mathrm{d}\hat{z} + \int_{0}^{\infty} [\rho_i(\hat{z}) - \rho_{i,\mathrm{vap}}]\mathrm{d}\hat{z} \quad (10)$$

where $\hat{z} = z - z_{\mathrm{Gibbs}}$ and $\rho_{i,\mathrm{liq}}$ is the bulk density of ions in the liquid phase, while $\rho_{i,\mathrm{vap}}$ denotes the corresponding one in the vapor phase; again, assuming that $\rho_{i,\mathrm{vap}} = 0$ is a good approximation. By convention, it is implied by eq 10 that the liquid phase of the mixture occupies the negative half-space ($\hat{z} < 0$) and the vapor phase the positive one ($\hat{z} > 0$). The condition of an overall electroneutrality of the solution implies that the adsorptions of anions and cations are the same, i.e., $\Gamma_i = \Gamma_{\mathrm{anion}} = \Gamma_{\mathrm{cation}} = \Gamma$. In our simulations, Γ_{anion} and Γ_{cation} agree within the range of the indicated error bars. We, therefore, report only the data for Γ, which we calculated as $\Gamma = (\Gamma_{\mathrm{anion}} + \Gamma_{\mathrm{cation}})/2$ in practice. The results we obtained for Γ from our simulation data are shown in Figures 6, 7, and 8 and will be discussed in detail in section 3.

The excess surface tension over that of the pure solvent, $\Delta\gamma(m)$, which is implied by the calculated adsorptions for different concentrations via integration of the Gibbs adsorption isotherm can be obtained as follows. Since we do not have any information about the activity coefficient of the ions in our simulations, we can only compute an "idealized" surface tension increment, $\Delta\gamma^{\mathrm{id}}$, using eq 11, which is based on eq 2. Within their respective error margins, the adsorptions Γ as derived from eq 1 and eq 2, respectively, using experimental surface tension data, are identical up to a concentration of $m \approx 1$ mol kg^{-1} (cf. Figures 6, 7, and 8 as well as ref 34). We are, therefore, confident that the surface tension increment $\Delta\gamma^{\mathrm{id}}$ will not differ much from the "true" value $\Delta\gamma$, which would be obtained if activity coefficients were taken into account, in this concentration range.

From the data for Γ at different concentrations, one interpolates the function $\Gamma(m)$ using a polynomial of sufficiently high degree to represent the available data faithfully (usually polynomials of second or third degree suffice), which is then integrated to yield the "idealized" excess (over that of pure water) surface tension $\Delta\gamma^{\mathrm{id}}$ at the target concentration m using eq 2

$$\gamma(m) - \gamma(0) = \Delta\gamma(m) \approx \Delta\gamma^{\mathrm{id}}(m) = -RT\int_0^m \frac{\Gamma(m)}{m}\mathrm{d}m \quad (11)$$

The predictions for the excess surface tension based on the adsorption data are compared to the data for $\Delta\gamma$ that have been calculated directly from the components of the pressure tensor in the simulation runs in section 3.

In addition to the adsorption and the surface tension, we have also evaluated the surface potential from the density profiles of water molecules and of ions. Since we use only nonpolarizable force fields, the total surface potential χ_{tot} can be calculated from the charge density alone[22,34]

$$\chi_{tot} = -\frac{1}{\varepsilon_0}\int_{z_{vap}}^{z_{liq}}\left(\int_{z_{vap}}^{z}\rho_q(z')dz'\right)dz \quad (12)$$

where ε_0 is the dielectric permittivity of vacuum and ρ_q denotes the total charge density, while z_{vap} and z_{liq} are arbitrary positions deep in the bulk vapor phase and in the bulk liquid phase, respectively. Of interest is also that part of the total surface potential which is caused by the preferential orientation of the dipole moment of water molecules near the surface, $\chi_{\mu,w}$

$$\chi_{\mu,w} = \frac{1}{\varepsilon_0}\int_{z_{vap}}^{z_{liq}}\rho_{\mu_z}(z)dz \quad (13)$$

where ρ_{μ_z} is the density of the z-component of the net dipole moment, which may be nonzero near the interface. While it was previously believed that eqs 12 and 13 should yield the same result for the liquid−vapor interface of pure water, it is now clear that eq 13 neglects quadrupolar contributions[54] generated by the charge distribution which are taken into account by eq 12. It is, nevertheless, sometimes instructive to investigate the dipolar part separately. Additionally, one may subdivide the total surface potential into a part caused by the water molecules, $\chi_{q,w}$, and another one due to the ion distribution, $\chi_{q,i}$, by separating the total charge density ρ_q according to the species which contribute to it ($\rho_q = \rho_{q,w} + \rho_{q,i}$). This separation is, however, somewhat artificial because the spatial distributions of ions and water molecules are not independent. Due to the additivity of the charge densities, the sum of the two contributions to the surface potential yields the total one: $\chi_{tot} = \chi_{q,w} + \chi_{q,i}$.

3. Results and Discussion

The density profiles for the cations (solid lines) and the anions (dashed lines) of aqueous solutions of NaF (OPLS force field) and NaI (OPLS and Koneshan et al. force fields) at different concentrations are shown in Figures 3−5. To facilitate deciding whether or not the ions are preferably adsorbed at the interface, the location of the Gibbs dividing surface in each case is indicated by a symbol (in order of increasing salt concentration: circle, square, diamond, triangle), which has been positioned—quite arbitrarily because the position z_{Gibbs} has a meaning only on the z-axis but not on the ρ-axis—at half the bulk density of the ions, $\rho_{i,liq}$, at the respective concentration (cf. Table 3). The density profiles of water are omitted from these plots for clarity.

The density profiles for NaF in Figure 3 show the usual classical behavior. As anticipated by Wagner[3] and by Onsager and Samaras[4] for small, hardly polarizable ions, both sodium and fluoride are effectively repelled from the interface. The profiles of cations and anions are almost identical and can be well described by simple hyperbolic-tangent functions of the form that was used to represent the water profile in eq 9 but replacing ρ_l by the bulk density $\rho_{i,liq}$ of the ion and z_{Gibbs} by the position $z_{0,i}$ at which, by symmetry, the ionic density reaches half its bulk value $\rho_{i,bulk}$. The absence of surface peaks and the shift of the inflection point of the ionic profile, $z_{0,i}$, with respect to the Gibbs dividing surface toward the liquid phase (cf. Table 3) imply a negative adsorption of the ions, which is shown as a function of the salt concentration in Figure 6.

TABLE 3: Distance $\hat{z}_{0,i} = z_{0,i} - z_{Gibbs}$ between the Gibbs Dividing Surface z_{Gibbs} and the Position $z_{0,i}$ at Which the Density of the Ionic Species i Reaches Half Its Bulk Value in the Liquid Phase ($\rho_{i,liq}$, Which Is Also Listed, Is the Same for Both Ionic Species) for Different Salts, Force Fields, and Concentrations m

NaF	OPLS		
m (mol kg^{-1})	$\hat{z}_{0,Na^+}$ (nm)	$\hat{z}_{0,F^-}$ (nm)	$\rho_{i,liq}$ (particles nm^{-3})
0.492	−0.475	−0.481	0.3273
0.984	−0.422	−0.447	0.6542
1.969	−0.427	−0.445	1.3215
3.845	−0.496	−0.493	2.6435
NaI	**OPLS**		
m (mol kg^{-1})	$\hat{z}_{0,Na^+}$ (nm)	$\hat{z}_{0,I^-}$ (nm)	$\rho_{i,liq}$ (particles nm^{-3})
0.508	−0.226	−0.055	0.3050
1.077	−0.190	−0.061	0.6288
2.215	−0.159	−0.069	1.2228
5.076	−0.115	−0.067	2.4509
NaI	**Koneshan et al.**		
m (mol kg^{-1})	$\hat{z}_{0,Na^+}$ (nm)	$\hat{z}_{0,I^-}$ (nm)	$\rho_{i,liq}$ (particles nm^{-3})
0.508	−0.268	−0.033	0.3038
1.077	−0.236	−0.037	0.6258
2.215	−0.188	−0.044	1.2122
5.076	−0.134	−0.051	2.4195

The density profiles as obtained from the OPLS force field for NaI at four different concentrations are shown in Figure 4. Two striking differences to the profiles for NaF in Figure 3 are to be noted. First, both types of ions approach the Gibbs dividing surface (marked again by symbols in the figure) much more closely, with the iodide ions (dashed lines) coming even closer than the sodium ions (solid lines), which are "dragged" to the surface by the iodide ions. This behavior is also reflected in the numbers of $z_{0,i}$ compiled for NaI in Table 3. Second, the profiles of cations and anions are no longer of the simple hyperbolic-tangent type observed for NaF. Instead, both profiles show a distinct surface structure. The density of iodide ions exhibits an enhancement near the surface, which is followed by a depletion as compared to the bulk density in a region in which the sodium density shows a peak. Estimating the sign of the net adsorption is, thus, less trivial than in the case of NaF, but on detailed evaluation of eq 10, Γ turns out to be negative for all concentrations (cf. Figure 7).

The density profiles obtained using the alternative force field by Koneshan et al.[43] for NaI, are shown in Figure 5. As in the case of the OPLS force field, the ions come much closer to the Gibbs dividing surface than in the solutions of NaF. The profiles and, consequently, also the net adsorptions (shown in Figure 8) are very similar to those obtained within the OPLS force field. At high salt concentrations, the surface enhancement for the iodide ions is even more pronounced than in the OPLS case.

From the density profiles in Figures 2−5, it is seen that our systems are big enough to show bulk behavior in the interior of the liquid phase, which is in accord with the estimates of Warren and Patel[35] who concluded that liquid slabs of at least 4−5 nm thickness are needed. The surface potentials and the adsorption of salt at the liquid−vapor interface can, therefore, be deduced reliably from our simulation data.

The results for the surface potentials of pure water and of the different salt solutions are compiled in Table 4. Shown are not only the total surface potentials χ_{tot} but also the contributions of the water molecules, $\chi_{q,w}$, and of the ions, $\chi_{q,i}$, separately. Additionally, the part of the surface potential which is due to

TABLE 4: Total Surface Potential χ_{tot}, Ionic Contribution $\chi_{q,i}$, Solvent Contribution $\chi_{q,w}$, and Dipolar Orientation Contribution of Water, $\chi_{\mu,w}$, for Pure Water and for the Salt Solutions of Concentration m Using the Indicated Force Fields

pure water	SPC/E (flexible)			
m (mol kg^{-1})	χ_{tot} (V)	$\chi_{q,i}$ (V)	$\chi_{q,w}$ (V)	$\chi_{\mu,w}$ (V)
---	−0.60	---	−0.60	+0.25
NaF	OPLS			
m (mol kg^{-1})	χ_{tot} (V)	$\chi_{q,i}$ (V)	$\chi_{q,w}$ (V)	$\chi_{\mu,w}$ (V)
0.492	−0.56	−0.79	+0.23	+1.03
0.984	−0.54	−0.58	+0.04	+0.84
1.969	−0.56	−0.87	+0.30	+1.13
3.845	−0.52	−0.86	+0.33	+1.18
NaI	OPLS			
m (mol kg^{-1})	χ_{tot} (V)	$\chi_{q,i}$ (V)	$\chi_{q,w}$ (V)	$\chi_{\mu,w}$ (V)
0.508	−0.52	+1.01	−1.53	−0.76
1.077	−0.54	+1.00	−1.54	−0.79
2.215	−0.56	+1.09	−1.65	−0.94
5.076	−0.52	+1.27	−1.80	−1.17
NaI	Koneshan et al.			
m (mol kg^{-1})	χ_{tot} (V)	$\chi_{q,i}$ (V)	$\chi_{q,w}$ (V)	$\chi_{\mu,w}$ (V)
0.508	−0.59	+1.67	−2.21	−1.44
1.077	−0.51	+1.75	−2.26	−1.54
2.215	−0.51	+1.77	−2.28	−1.59
5.076	−0.48	+1.89	−2.36	−1.75

the preferential orientation of the permanent dipole moment of water molecules near the interface, $\chi_{\mu,w}$, is listed. The contribution of this part to the total surface potential is already accounted for by $\chi_{q,w}$, which, in addition, contains the contributions of higher moments generated by the charge distribution.[54]

The values of $\chi_{tot} = -0.60$ V and $\chi_{\mu,w} = +0.25$ V for pure water within the flexible SPC/E model are in good agreement with the results of Sokhan and Tildesley[54] for the rigid version of this model: $\chi_{tot} = -0.55$ V and $\chi_{\mu,w} = +0.21$ V. The difference between $\chi_{tot} = \chi_{q,w}$ and $\chi_{\mu,w}$ demonstrates the importance of the contribution of higher electric moments to the surface potential. The above data are also in reasonable agreement with the results for χ_{tot} for polarizable water models. Ishiyama and Morita report a value of $\chi_{tot} = -0.42$ V and conclude that polarizability (by means of induced dipole moments) yields only a small contribution to the total surface potential.[34]

When comparing the surface potentials of the different salt solutions, the first striking observation is that the total value, χ_{tot}, is almost independent of the salt and its concentration. It remains in the range between −0.5 and −0.6 V. That the surface potential is, indeed, rather insensitive to the salt concentration has also been found in experiments.[6] As already noted by Ishiyama and Morita,[34] this approximate constancy of χ_{tot} is the result of a cancelation of two effects, which can be separated in the simulation. Furthermore, this separation demonstrates the difference between the solutions of NaF and those of NaI. For the former, the ionic contribution $\chi_{q,i}$ is negative, while for the latter, it is positive (cf. Table 4). The opposite is true for the contribution of water molecules to the surface potential, $\chi_{q,w}$; while $\chi_{q,w}$ is small, but positive, for solutions of NaF, it is relatively large and negative for the NaI solutions. More illuminating in terms of the molecular mechanism causing these numerical values is perhaps the comparison of the dipolar part

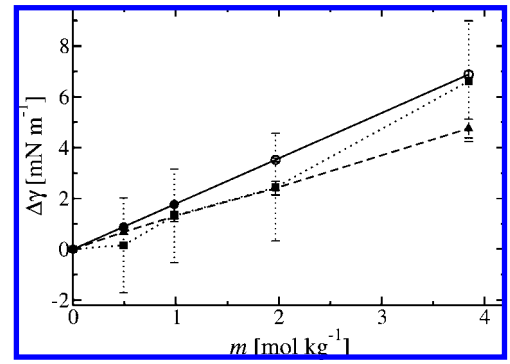

Figure 9. Excess surface tension $\Delta\gamma$ for NaF as a function of molality m. Shown are the experimental data of Matubayasi et al.[13] (filled circles), which are extrapolated beyond the solubility limit of $m = 1$ mol kg^{-1} (indicated by open circles) and connected by a solid line. The values for $\Delta\gamma$ obtained in the simulations are shown as squares connected by a dotted line. The data calculated from the adsorption according to eq 11 are represented as triangles and connected by a dashed line.

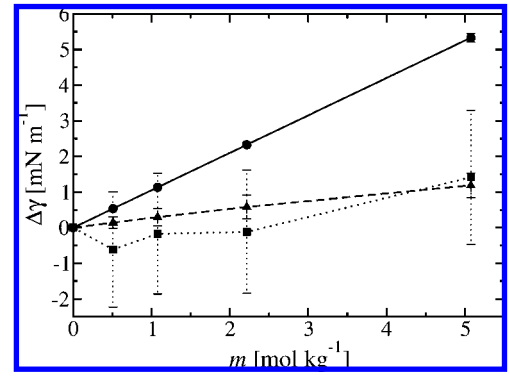

Figure 10. Excess surface tension $\Delta\gamma$ for NaI (OPLS potential) as a function of molality m. Shown are the experimental data of Matubayasi et al.[13] (circles), which are extrapolated beyond $m = 1$ mol kg^{-1} (solid line). The values for $\Delta\gamma$ obtained in the simulations are shown as squares connected by a dotted line; the data calculated from the adsorption according to eq 11 are represented as triangles and connected by a dashed line.

of the surface potential, $\chi_{\mu,w}$, which indicates the preferential orientation of the water dipole with respect to the z-axis. Close to the interface of pure water, on the liquid side, there is a slight tendency for the z-component of the dipole moment to point toward the liquid region.[54] This trend is strongly enhanced in solutions of NaF, while in solutions of NaI, the dipole is preferentially oriented toward the vapor phase in the vicinity of the interface. This behavior is caused by the formation of an electric double layer due to the spatial separation of anions and cations. The anions are found closer to the surface than the cations, and since the water dipoles in solution tend to point toward the anions they, consequently, show a preferential orientation toward the vapor phase, which changes the sign of $\chi_{\mu,w}$ as compared to pure water and the solutions of NaF. These findings are in complete agreement with the conclusions of Ishiyama and Morita.[34]

The adsorption and surface tension data, as obtained from our simulations, are compared with experimental data in Figures 6−11. The primary sources of data in this respect are measurements of the surface tension. In all cases, the increase of γ with increasing concentration m is found to be linear.[2,6,13] For the slope, Matubayasi et al.[13] report $d\gamma/dm = (1.79 \pm 0.035)$ mN m^{-1} kg mol^{-1} for NaF at 298 K in the concentration range from 0 to 1 mol kg^{-1}, which marks the solubility limit for this salt. A correlation of their experimental surface tension data obtained

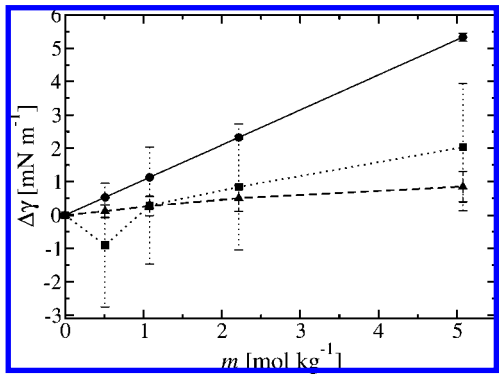

Figure 11. Excess surface tension $\Delta\gamma$ for NaI (Koneshan et al. force field) as a function of molality m. Shown are the experimental data of Matubayasi et al.[13] (circles), which are extrapolated beyond $m = 1$ mol kg^{-1} (solid line). The values for $\Delta\gamma$ obtained in the simulations are shown as squares connected by a dotted line; the data calculated from the adsorption according to eq 11 are represented as triangles and connected by a dashed line.

in the same concentration range for solutions of NaI, which is soluble up to 12 mol kg^{-1}, yields $d\gamma/dm = (1.05 \pm 0.023)$ mN m^{-1} kg mol^{-1}. We do not hesitate to extrapolate $\Delta\gamma$ to higher concentrations linearly—this prodecure is not very meaningful for real NaF, of course, but our model NaF (OPLS force field) turns out to be much more soluble than the real one. This enhanced solubility is a combined effect of using an imperfect force field, which does not reproduce all aspects of aqueous solutions of NaF properly, and of the finite size of the simulation, both in space and in time. This kinetic effect would suppress the crystallization of NaF out of the supersaturated solution for a long time even if a perfect force field was available. For NaI, there are experimental data available for higher concentrations,[6] and they are found to be consistent with our extrapolation of Matubayasi's data. We use these surface tension data in conjunction with experimentally determined activity coefficients[42] to obtain the experimental adsorptions as outlined in section 2.2.

The adsorption data for NaF are shown in Figure 6 as a function of molality. The circles (connected by a continuous line to guide the eye) represent the experimental adsorption data Γ deduced from the surface tension measurements of Matubayasi et al.[13] using experimental activity coefficient data,[42] while the squares (connected by a dotted line) are the "idealized" adsorption data obtained using eq 2 instead of eq 1, i.e., when neglecting activity coefficients by setting $f = 1$ throughout. Reasonably good agreement between the two sets is found up to the solubility limit of NaF at a concentration of 1 mol kg^{-1}. Beyond it, we can only extrapolate the idealized adsorption linearly. The results of our simulations are denoted by triangles (connected by the dashed line). It is seen that the simulated adsorption decreases nearly linearly, as the experimental data do, but the adsorption in the simulated system is not as pronounced (not as negative) as in the real one.

The excess surface tension $\Delta\gamma$ for NaF as a function of molality is displayed in Figure 9. The circles, connected by the continuous line, represent the experimental results of Matubayasi et al.[13] (filled circles), extrapolated linearly for $m > 1$ mol kg^{-1} (open circles) to be able to compare to our simulation data, although this concentration range is beyond the solubility limit of real NaF.[42] The results that we obtained directly from our simulations via the difference of the lateral and the normal components of the pressure (eq 4) are denoted by squares which are connected by a dotted line. For the calculation of $\Delta\gamma^{id}$ from our simulated adsorption data using eq 11, the data represented by triangles and connected by a dashed line are obtained. The surface tension data that were calculated in the two different ways agree within their error margins, but the ones obtained from the adsorption are smoother and have smaller error bars. The surface tension increment which is taken directly from the simulation is quite noisy. Typically, the uncertainty of the surface tension data obtained via the adsorption is less than 0.5 mN m^{-1}, which is to be compared with an error of 1.5 mN m^{-1} in the directly calculated values. Both calculated surface tensions are smaller than the experimental values, which is in line with the adsorption data (cf. Figure 6) whose magnitude turns out to be underestimated by the simulations. When comparing the excess surface tension obtained from the simulations to the calculated $\Delta\gamma^{id}$, it should be kept in mind that the condition $f \gg m df/dm$ may no longer be fulfilled for $m \geq 2$ mol kg^{-1}, and the neglect of the concentration dependence of the activity coefficient becomes a serious issue.

The corresponding adsorption data for NaI as a function of the concentration are shown and compared to the simulation results obtained using the OPLS potential for the ions in Figure 7. The adsorptions Γ deduced from the experimental surface tension data of Matubayasi et al.[13] using experimental activity coefficients[42] are represented by circles (continuous line), while the ones that neglect the activity coefficients are shown as squares and connected by the dotted curve. The simulation results are denoted by triangles and connected by the dashed curve. As in the case of NaF, the simulated adsorption data are not as negative as the experimental ones. It should be noted, however, that the adsorption of NaI is negative for all concentrations despite the visible surface peak in the density profile (cf. Figure 4).

Figure 10 displays the experimental excess surface tension of NaI and compares it to the simulation results obtained within the OPLS model for the ions. Matubayasi's data[13] are represented by circles (connected by a continuous line); they have been extrapolated beyond 1 mol kg^{-1}, but agree with the surface tension data reported by Jarvis and Scheiman[6] in the concentration range shown. The simulated excess surface tension obtained directly from the pressure anisotropy is represented as squares connected by a dotted line, while the corresponding data that were derived from the simulated adsorption using eq 11 are shown as triangles (dashed line). As in the case of NaF, the two sets of calculated surface tensions agree within the range of their uncertainties, but the set derived from the adsorption data is more consistent and less error-prone. The directly simulated surface tension increments are found to be negative over a relatively wide concentration range, in which the adsorption itself is negative. This thermodynamic contradiction gives us an idea of the considerable uncertainty of the directly calculated simulation data, which is usually about 1.5 mN m^{-1}. It should be stressed, however, that positive values of $\Delta\gamma$ are within the limits of the error margin in all cases. The calculated increase of the surface tension is much smaller than the experimentally observed one, as was to be expected from the adsorption data, the magnitude of which the simulations vastly underestimate (cf. Figure 7).

In view of the mediocre performance of the OPLS force field for NaI, we employed another NaI potential, derived by Koneshan et al. (cf. Table 1),[43] to check the dependence of the results for the adsorption and the excess surface tension on the details of the force field. The results are shown in Figures 8 and 11, respectively. The meaning of the symbols is the same as in Figures 7 and 10, but the simulated data were obtained

using the new force field. It is seen in Figure 8 that the force field of Koneshan et al. yields similar results for the adsorption as the OPLS. As in both before-mentioned cases, the directly simulated data for the surface tension increment $\Delta\gamma$ (cf. Figure 11) and the ones derived from the adsorption data using eq 11 agree within their respective error margins, but the route via the adsorption generally yields more accurate and more reliable results.

4. Conclusion

The liquid−vapor interfaces of aqueous solutions of NaF and NaI have been simulated for different salt concentrations using nonpolarizable force fields for both ions (OPLS and, additionally for NaI, a force field developed by Koneshan et al.) and water molecules (represented by a flexible SPC/E model). From the density profiles of the different species, we obtained the adsorption of the salt to the interface and the excess surface tension over that of pure water. The results for the latter quantity were compared to the data for the surface tension increment obtained directly from the simulations via the pressure anisotropy.

Our results for the NaF solutions are as it was to be expected from the classical picture of interfaces of salt solutions: Both types of ions are repelled from the liquid−vapor interface, forming a depletion layer at the surface and, thus, leading to an increase of the surface tension as compared to pure water. That both (negative) adsorption and (positive) surface tension increment turn out to be too small in magnitude to reproduce the experimental data indicates that there is room for improvement with regard to the force field for this mixture.

For solutions of NaI, the results are more complex than the simple classical view suggests. We employed two different nonpolarizable force fields, one based on OPLS parameters, the other one as derived by Koneshan et al. The OPLS force field produces a small enhancement of the iodide concentration near the surface (much smaller than the one Jungwirth and Tobias[11] observed for their polarizable force field) and, consequently, predicts only a slightly negative adsorption. The excess surface tension is largely underestimated compared to the experimental data. The findings for the Koneshan et al. force field are similar to those obtained within the OPLS. As in the case of NaF, there is clearly the possibility to improve the force field with respect to reproducing the experimental adsorption and the surface tension data more accurately.

An important finding in our simulations and subsequent calculations is that the excess of the surface tension over that of the pure solvent is more reliably obtained from the adsorption of the solute to the interface, which is accessible through the density profiles via eq 11, than from direct evaluation of the lateral and normal components of the pressure tensor (Kirkwood−Buff equation) during the simulations. It is reassuring that the results of the two methods are in agreement with each other in the boundaries set by their respective error margins, but the detour via the adsorptions yields more consistent results and smaller errors (by a factor of 3) even in the absence of a detailed knowledge of the activity coefficients in the simulated systems (for not too high concentrations, at least, i.e., for $m < 2$ mol kg^{-1}).

After it has been established that the relationship between adsorption and excess surface tension implied by the Gibbs adsorption isotherm and, thus, following from the first and second laws of thermodynamics is, in all likelihood, not violated even in simulations but can actually be taken advantage of in calculating the surface tension more accurately, a few possible directions of future research should be mentioned here. It is evident that several different force fields can be devised to reproduce one or more of the following quantities of interest: adsorption, surface tension, and concentration of ions right at the interface. While probably no existing force field has been optimized with respect to these interfacial properties, one important aspect in improving our current potential models is to decrease the adsorption, making it more negative and, at the same time, to increase the surface tension increment. In apparent contradiction to these features, the surface peak of the halide anion should be more pronounced than in our simulations to be able to obtain the presence of ions at the surface which, in turn, is needed to rationalize the kinetics of certain reactions taking place at the liquid−gas boundary.[7,8] The polarizable models used by Jungwirth and Tobias[11] successfully produce such an enhanced surface concentration while giving an increase of the surface tension, but nothing is known about the net adsorption in these simulations. As we have shown here, much larger systems than hitherto studied in simulations of polarizable models must be considered to achieve true bulk behavior in the liquid phase. Investigations of the consistency of net adsorption and excess surface tension for these supposedly superior, but computationally more demanding polarizable potential models are therefore highly desirable.

Acknowledgment. We would like to thank Malte Kleemeier for helping us to retrieve experimental data for the densities of salt solutions. Financial support from the German Research Foundation (Deutsche Forschungsgemeinschaft) through grant WE 2540/3-2 is gratefully acknowledged. Daniel dos Santos expresses his gratitude to the Portuguese Science Foundation (Fundaçao para a Ciencia e a Tecnologia) for the postdoctoral research grant SFRH/BPD/1815/2004.

Appendix

Thermodynamic Foundation of the Gibbs Adsorption Isotherm. Being the surface analog of the Gibbs−Duhem relation for a single bulk phase, the Gibbs adsorption isotherm follows directly from the combination of the first and second laws of thermodynamics (a fundamental equation) for a system containing at least two phases and an interface between them. It establishes a connection between the adsorption of the solute to this interface and the change of the surface tension of the solution.[30] Consider a system containing two phases (liquid and vapor, for example) of a binary mixture of, say, water (w) and solute (s), the latter being salt in our case. At constant temperature, an infinitesimal change in the surface Gibbs free energy G^σ is given by

$$dG^\sigma = \gamma dA + \mu_w dn_w^\sigma + \mu_s dn_s^\sigma \tag{14}$$

where γ denotes the surface tension and A the interfacial area, while μ_i is the chemical potential of species $i \in \{w, s\}$ and n_i^σ expresses the number of particles i in the interfacial region which are present *in excess* over the total number of particles i in the bulk vapor and bulk liquid phases that would be counted if there was a sharp boundary between these two phases and each phase had its bulk composition up to this hypothetical boundary. In the real interfacial region, however, the particle densities vary smoothly, and it is important to note that n_i^σ can be positive or negative because species i may be enriched or depleted in the interfacial region. Obviously, the values of n_i^σ depend on where exactly the hypothetical boundary (the dividing surface between liquid and vapor) is placed, and it should also be clear that n_w^σ and n_s^σ both vary *according to this choice*, i.e., not independently.

The total surface Gibbs free energy at constant temperature can be written as

$$G^\sigma = \gamma A + \mu_w n_w^\sigma + \mu_s n_s^\sigma \quad (15)$$

Subtracting the formal total differential of G^σ

$$dG^\sigma = \gamma dA + A d\gamma + \mu_w dn_w^\sigma + n_w^\sigma d\mu_w + \mu_s dn_s^\sigma + n_s^\sigma d\mu_s \quad (16)$$

from eq 14 yields one version of the Gibbs adsorption isotherm

$$0 = A d\gamma + n_w^\sigma d\mu_w + n_s^\sigma d\mu_s \quad (17)$$

It is customary to divide this equation by the interfacial area A and to introduce the adsorption (also referred to as the surface excess) $\Gamma_i = n_i^\sigma / A$ of species i. The Gibbs adsorption isotherm can then be cast into the form

$$d\gamma = -\Gamma_w d\mu_w - \Gamma_s d\mu_s \quad (18)$$

By convention, the Gibbs dividing surface, which, once again, is a mathematical construct of a hypothetical sharp boundary between liquid and vapor phase, is located in such a way that the adsorption Γ_w of the solvent (water) becomes zero. This particular choice of the Gibbs dividing surface is also called the equimolar surface. Once this conceptual boundary between the phases, which replaces the mathematically vague term "interfacial region", has been fixed in space, the adsorption of the solute $\Gamma_s \equiv \Gamma$ is uniquely defined and can be calculated according to eq 10. Using $d\mu_s = RT\, d \ln a$ at constant temperature, where the activity of the solute, a_s, is denoted by a for notational simplicity, the Gibbs adsorption isotherm $d\gamma = -\Gamma_s d\mu_s$ (with $\Gamma_w = 0$) can be represented in the form given by eq 1.

References and Notes

(1) Heydweiller, A. *Ann. Phys.* **1910**, *33*, 145.
(2) Weissenborn, P. K.; Pugh, R. J. *J. Colloid Interface Sci.* **1996**, *184*, 550.
(3) Wagner, C. *Phys. Z.* **1924**, *25*, 474.
(4) Onsager, L.; Samaras, N. N. T. *J. Chem. Phys.* **1934**, *2*, 528.
(5) Levin, Y. *J. Chem. Phys.* **2000**, *113*, 9722.
(6) Jarvis, N. L.; Scheiman, M. A. *J. Phys. Chem.* **1968**, *72*, 74.
(7) Hu, J. H.; Shi, Q.; Davidovits, P.; Worsnop, D. R.; Zahniser, M. S.; Kolb, C. E. *J. Phys. Chem.* **1995**, *99*, 8768.
(8) Knipping, E. M.; Lakin, M. J.; Foster, K. L.; Jungwirth, P.; Tobias, D. J.; Gerber, R. B.; Dabdub, D.; Finlayson-Pitts, B. J. *Science* **2000**, *288*, 301.
(9) Jungwirth, P.; Tobias, D. J. *J. Phys. Chem. B* **2000**, *104*, 7702.
(10) Perera, L.; Berkowitz, M. L. *J. Chem. Phys.* **1994**, *100*, 3085.
(11) Jungwirth, P.; Tobias, D. J. *J. Phys. Chem. B* **2001**, *105*, 10468.
(12) Garrett, B. C. *Science* **2004**, *303*, 1146.
(13) Matubayasi, N.; Tsunetomo, K.; Sato, I.; Akizuki, R.; Morishita, T.; Matuzawa, A.; Natsukari, Y. *J. Colloid Interface Sci.* **2001**, *243*, 444.
(14) Liu, D.; Ma, G.; Levering, L. M.; Allen, H. C. *J. Phys. Chem. B* **2004**, *108*, 2252.
(15) Raymond, E. A.; Richmond, G. L. *J. Phys. Chem. B* **2004**, *108*, 5051.
(16) Petersen, P. B.; Saykally, R. J. *J. Phys. Chem. B* **2006**, *110*, 14060.
(17) Ghosal, S.; Hemminger, J. C.; Bluhm, H.; Mun, B. S.; Hebenstreit, E. L. D.; Ketteler, G.; Ogletree, D. F.; Requejo, F. G.; Salmeron, M. *Science* **2005**, *307*, 563.
(18) Padmanabhan, V.; Daillant, J.; Belloni, L.; Mora, S.; Alba, M.; Konovalov, O. *Phys. Rev. Lett.* **2007**, *99*, 086105.
(19) Kim, J.-H.; Kim, Y.-K.; Kang, H. *J. Phys. Chem. C* **2007**, *111*, 8030.
(20) Dang, L. X.; Chang, T.-M. *J. Phys. Chem. B* **2002**, *106*, 235.
(21) Dang, L. X. *J. Phys. Chem. B* **2002**, *106*, 10388.
(22) Chang, T.-M.; Dang, L. X. *Chem. Rev.* **2006**, *106*, 1305.
(23) Vrbka, L.; Mucha, M.; Minofar, B.; Jungwirth, P.; Brown, E. C.; Tobias, D. J. *Curr. Opin. Colloid Interface Sci.* **2004**, *9*, 67.
(24) Patra, M.; Karttunen, M. *J. Comput. Chem.* **2004**, *25*, 678.
(25) Bhatt, D.; Newman, J.; Radke, C. J. *J. Phys. Chem. B* **2004**, *108*, 9077.
(26) Bhatt, D.; Chee, R.; Newman, J.; Radke, C. J. *Curr. Opin. Colloid Interface Sci.* **2004**, *9*, 145.
(27) Kalra, A.; Tugcu, N.; Cramer, S. M.; Garde, S. *J. Phys. Chem. B* **2001**, *105*, 6380.
(28) Pal, S.; Müller-Plathe, F. *J. Phys. Chem. B* **2005**, *109*, 6405.
(29) Eggimann, B. L.; Siepmann, J. I. *J. Phys. Chem. C* **2008**, *112*, 210.
(30) Rowlinson, J. S.; Widom, B. *Molecular Theory of Capillarity*; Clarendon: Oxford, 1982.
(31) Jungwirth, P.; Tobias, D. J. *Chem. Rev.* **2006**, *106*, 1259.
(32) Mucha, M.; Frigato, T.; Levering, L. M.; Allen, H. C.; Tobias, D. J.; Dang, L. X.; Jungwirth, P. *J. Phys. Chem. B* **2005**, *109*, 7617.
(33) Jungwirth, P.; Tobias, D. J. *J. Phys. Chem. B* **2002**, *106*, 6361.
(34) Ishiyama, T.; Morita, A. *J. Phys. Chem. C* **2007**, *111*, 721.
(35) Warren, G. L.; Patel, S. *J. Phys. Chem. C* **2008**, *112*, 7455.
(36) For a calculation of the excess surface tension from the adsorption of sodium halides near hydrophobic self-assembled monolayers, see: Horinek, D.; Netz, R. R. *Phys. Rev. Lett.* **2007**, *99*, 226104.
(37) van der Spoel, D.; Lindahl, E.; Hess, B.; Groenhof, G.; Mark, A. E.; Berendsen, H. J. C. *J. Comput. Chem.* **2005**, *26*, 1701.
(38) Åqvist, J. *J. Phys. Chem.* **1990**, *94*, 8021.
(39) McDonald, N. A.; Duffy, E. M.; Jorgensen, W. L. *J. Am. Chem. Soc.* **1998**, *120*, 5104.
(40) Chandrasekhar, J.; Spellmeyer, D. C.; Jorgensen, W. L. *J. Am. Chem. Soc.* **1984**, *106*, 903.
(41) Söhnel, O.; Novotný, P. *Densities of aqueous solutions of inorganic substances*; Elsevier: Amsterdam, 1985.
(42) Lide, D. R., Ed. *CRC Handbook of Chemistry and Physics*, 82nd ed.; CRC Press: Boca Raton, FL, 2001.
(43) Koneshan, S.; Rasaiah, J. C.; Lynden-Bell, R. M.; Lee, S. H. *J. Phys. Chem. B* **1998**, *102*, 4193.
(44) Berendsen, H. J. C.; Grigera, J. R.; Straatsma, T. P. *J. Phys. Chem.* **1987**, *91*, 6269.
(45) Wallqvist, A.; Teleman, O. *Mol. Phys.* **1991**, *74*, 515.
(46) Miyamoto, S.; Kollman, P. A. *J. Comput. Chem.* **1992**, *13*, 952.
(47) Nosé, S. *Mol. Phys.* **1984**, *52*, 255.
(48) Hoover, W. G. *Phys. Rev. A* **1985**, *31*, 1695.
(49) Darden, T.; York, D.; Pedersen, L. *J. Chem. Phys.* **1993**, *98*, 10089.
(50) Essmann, U.; Perera, L.; Berkowitz, M. L.; Darden, T.; Lee, H.; Pedersen, L. G. *J. Chem. Phys.* **1995**, *103*, 8577.
(51) Chen, F.; Smith, P. E. *J. Chem. Phys.* **2007**, *126*, 221101.
(52) Orea, P.; López-Lemus, J.; Alejandre, J. *J. Chem. Phys.* **2005**, *123*, 114702.
(53) Alejandre, J.; Tildesley, D. J.; Chapela, G. A. *J. Chem. Phys.* **1995**, *102*, 4574.
(54) Sokhan, V. P.; Tildesley, D. J. *Mol. Phys.* **1997**, *92*, 625.

JP804811U